Freezing-Memory Effect of Water on Nucleation of CO_2 Hydrate Crystals

Satoshi Takeya*

Graduate School of Environmental Earth Science, Hokkaido University, N10 W5, Sapporo 060-0510, Japan

Akira Hori and Takeo Hondoh

Institute of Low Temperature Science, Hokkaido University, N19 W8, Sapporo 060-0819, Japan

Tsutomu Uchida

Hokkaido National Industrial Research Institute,2-17 Tukisamu Higashi Toyohira-ku, Sapporo 062-8517, Japan

Received: October 21, 1999; In Final Form: February 4, 2000

We measured the times to nucleate CO_2 hydrates from CO_2 dissolved water under pressure and 8.6 K supercooling using different methods to prepare the water. These times ranged from 50 min to more than 7200 min, depending on the preparation method. The nucleation rates were calculated by fitting the observed nucleation probability distributions to a nucleation rate equation. The nucleation rates significantly increased when the water had previously frozen as ice and melted (freezing-memory effect), except when the meltwater was heated to 298 K before nucleation. The nucleation rates also increased with O_2-saturated meltwater, but decreased with degassed water.

I. Introduction

Gas hydrates are ice-like inclusion compounds formed from gas and water molecules. Stackelberg and Muller[1,2] determined two of their crystal structures. The cages are hydrogen bonded water molecules that form 12- and 14-hedrons in structure I (space group *Pm*3*n*), and 12- and 16-hedrons in structure II (space group *Fd*3*m*). However, due to the difficulty of quantifying kinetic phenomena, little is known about their nucleation and growth mechanisms.

Bishnoi and co-workers[3,4] measured nucleation times (induction times) for CH_4 hydrate and found they depended on the history of the water sample. Hwang et al.[5] experimented with definite gas−water interfacial surface areas under quiescent conditions and found that CH_4 hydrates nucleated from meltwater, but not from liquid water that had not been previously frozen. They concluded that meltwater provides a template for hydrate nucleation. Additionally, residual structures after hydrate decomposition were investigated by viscosity changes[6] and $p-T$ hysteresis.[7] These studies advocated two kinds of memory effects, those from meltwater and those from dissociated hydrate, although neither was examined quantitatively. However, memory effects from the container of the fluids cannot be ruled out.

Recently, Benmore et al.[8] measured neutrons diffracted from tetrabutylanmonium choloride in deuterated water and found no significant difference in the total structure among mixtures with different thermal histories after dissociation. However, only one microscopic nucleus can significantly change the nucleation time, which would not be detected; hence, this neutron diffraction study is suggestive, not conclusive.

We measured the induction times for CO_2 hydrate from meltwater and from water not previously frozen, hereafter called nontreated water. Nucleation was detected by the rise in temperature. To average out statistical fluctuations,[9] we made ten measurements per water sample to estimate the nucleation rates. The nucleation rate from meltwater was an order of magnitude larger than that from nontreated water. In addition, we investigated the effects of degassing, O_2 saturation, N_2 saturation, and CO_2 saturation on the nucleation rate. We also detected CO_2 hydrate crystals using energy-dispersive X-ray diffraction.

II. Experimental Section

a. High-Pressure Apparatus for X-ray Diffraction. Figure 1a is a schematic of the experimental apparatus. The cylindrical high-pressure cell is made of duralumin (Al, Cu−Mn−Mg−Si alloy) and was fixed on the four-circle goniometer. The inner diameter and the thickness of the high-pressure cell were 11.0 mm and 2.0 mm, respectively. For diffraction profile measurements, a high-energy X-ray generator (Rigaku model HVR-200) with a W-target was operated at 185 kV × 90 mA, and a Cd−Zn−Te energy-dispersive detector (AMP-TEC model XR-100T-CZT) was used. The X-ray transmissivity of the high-pressure cell was 30% at 20 keV, 76% at 60 keV, and 84% at 100 keV. Energy dispersive spectra were measured by the detector and a multichannel analyzer (Rigaku model MCA2). The incident X-ray beam was collimated by a long, stainless steel sleeve with a 0.40 × 2.00 × 110-mm^3 slit, and the diffracted X-ray beam was also defined by two 0.40-mm wide line slits to remove diffraction by the cell (Figure 1b). The diffraction angle 2θ was fixed at 5.00 degrees so that low index diffraction peaks of structure I hydrate appeared in a high transmissivity range (40−60 keV). The diffraction spectra accumulated continuously in the computer memory, but the data were retrieved every 3600 s because of very weak diffraction intensities.

The pressure in the sample cell was measured by a pressure sensor (Kyowa Electronic Instruments model PG-200KU) and was kept constant by a pressure-reducing valve. Fluctuation in

* Corresponding author. E-mail: takeya@hhp2.lowtem.hokudai.ac.jp. Fax: +81-11-706-7351.

10.1021/jp993759+ CCC: $19.00
Published on Web 04/07/2000

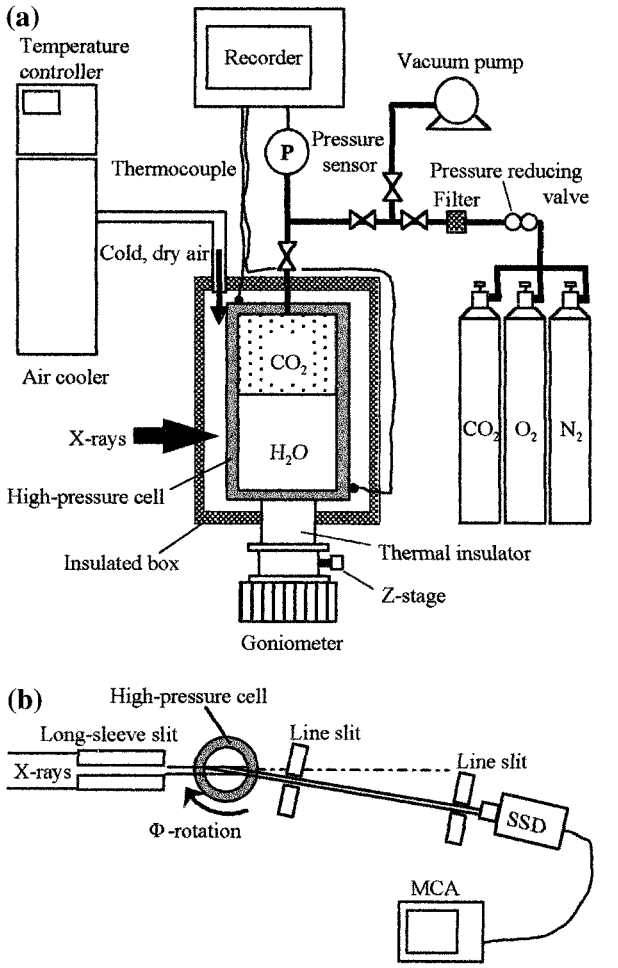

Figure 1. (a) High-pressure apparatus for X-ray diffraction. (b) Energy-dispersive X-ray diffraction layout.

the pressure was ± 0.04 MPa at the applied pressure of 4.7 MPa. A cold, dry airflow cooled the sample cell and the temperature was measured by two thermocouples attached on the outside of the cell. A heater installed in the air inlet pipe controlled the temperature to ±0.1 K and the temperature difference measured by the two thermocouples was ±0.1 K. Although the temperature in the cell was not measured during experiments, it was calibrated to that measured on the outside of the cell by measuring the temperature in the cell without pressurization before the experiments. This calibration was done with and without melting ice. The temperature hereafter is this calibrated and averaged temperature.

b. Procedure. To clarify the freezing-memory effect, we tried several different treatments of the water samples. First, 1.0 mL of ultrapure water (Millipore 18.3 MΩ-cm, Milli-Q SP Toc) was put into the high-pressure cell, and then the different preparations listed below were made for the different water samples. After each measurement, the water was always replaced by fresh ultrapure water and the high-pressure cell was rinsed.

(1) The temperature of the water sample was kept at 275.0 K for 60 min in the cell. We designate this water as nontreated water.

(2) The temperature of the water sample was reduced to 258.0 K. Freezing was confirmed by the temperature rise. Then the temperature was kept at 258.0 K for 30 min to completely freeze the water sample. During the subsequent heating, melting was detected when the temperature ceased rising at 273.1 K for about 10 min owing to the latent heat of melting. Then, the temperature increased to the reaction temperature 275.0 K. The water sample

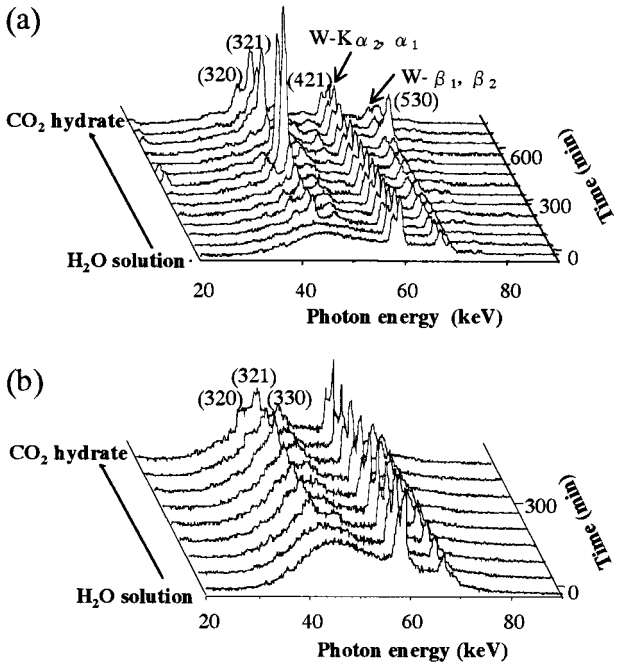

Figure 2. Energy-dispersive X-ray diffraction profiles during growth of CO_2 hydrate at 4.9 MPa, 274 K. (a) No rotation of the high-pressure cell. (b) 90° rotation about ϕ-axis during the measurement.

remained at the reaction temperature for 2 h to melt the ice completely. We designate this water as meltwater.

(3) Vacuum was drawn on the nontreated water sample, given in procedure (1), for 900 s at 275.0 K using an oil-free vacuum pump (Iwaki Glass model FTP-10A). We designate this water sample degassed water.

(4) Vacuum was drawn on another water sample for 900 s at 275.0 K and during the cool-down to 258.0 K. This water was frozen and melted by the procedure described in (2) and is designated degassed meltwater.

(5) To look for possible effects from O_2, N_2, and CO_2, we also used O_2-saturated meltwater, N_2-saturated meltwater, and CO_2-saturated meltwater. After drawing vacuum for 900 s at 275.0 K, O_2 gas (Daido-Hoxan, purity 99.5 vol %; less than 0.5 vol % of N_2, Ar, and CH_4), N_2 gas (Daido-Hoxan, purity 99.99 vol %), or CO_2 gas (Daido-Hoxan, purity 99.5 vol %; less than 0.5 vol % of N_2, O_2, H_2, and CH_4) was passed through the 0.5-μm membrane filter and into the cell. O_2 and N_2 gas were passed until the pressure reached 5.0 MPa, and CO_2 gas reached only 1.0 MPa to avoid exceeding the CO_2 hydrate formation pressure. These pressures were then held for 5 h, and the pressure was decreased to 0.1 MPa to obtain the gas-saturated water samples. They were then processed by the same procedure as (2).

After each procedure, the whole apparatus was evacuated by the vacuum pump for 10 s. Then CO_2 (purity given in (5)) was slowly introduced through a 0.5-μm membrane filter (NUPRO model SS-2F−T7−05) into the cell. The pressure increased for 900 s until reaching 4.7 MPa. During this procedure, the temperature in the cell increased by about 2 K maximum, but thereafter was kept constant at 275.0 ± 0.1 K (274.2 ± 0.1 K at the thermocouple) after the gas introduction, except during crystallization (Figure 4).

III. Results

a. Formation Process of CO_2 Hydrate. Formation of the hydrate crystals was confirmed by X-ray diffraction profiles as shown in Figure 2a,b. Although only three or four diffraction

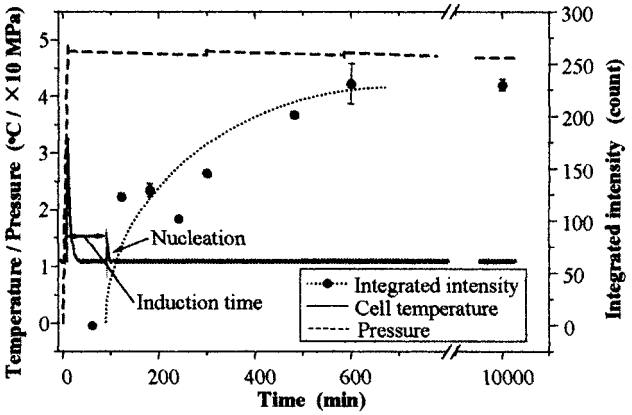

Figure 3. The temperature and pressure profile of the high-pressure cell and the integrated intensity of the (321) diffraction. The first and second peaks in the temperature profile are due to the admission of liquid CO_2 and the CO_2 hydrate nucleation, respectively. The integrated intensities are plotted at the time when each measurement for 3600 s was finished. The error bar of the intensity on the *y*-axis denotes the error of integrated intensity by Gauss fitting.

peaks were distinguished (because of weak diffraction intensities), the peaks fit those of structure I with a lattice constant of 12.00 Å. As reported by Koh et al.,[10] we also observed a large fluctuation in their intensities as a function of time (Figure 2a). However, this fluctuation vanished when the sample cell was rotated gradually about the vertical axis by 90 degrees during the intensity measurements as shown in Figure 2b. Having only a few crystals that satisfied the diffraction condition might have caused this fluctuation. In addition, individual diffraction spots were observed in Laue photographs taken in front of the second line slit.

The intensity of the (321) diffraction peak in Figure 2b was plotted against the reaction time in Figure 3. In this plot, the integrated intensity was calculated for each point by subtracting the broad peak due to the liquid phase as a background correction. The intensity abruptly increased roughly simultaneously with the exothermal peak in the temperature record, and then gradually leveled off. Although measurements continued for up to 7 days, no increase in intensity was measured after 10 h. The exothermal event had an abrupt temperature increase by about 1 K followed by a slow decrease for several minutes.

Hydrate formation at the same temperature and pressure as in the previous experiments was also observed using a CCD camera and a transparent high-pressure cell[11] under quiescent conditions. The formation process is illustrated in Figure 4. Nucleation occurred near the CO_2−water boundary after about 40 min. Within a second, a thin hydrate film grew from the vessel wall and spread across the CO_2−water boundary. Then, many needle-like crystals grew downward from the boundary and fell off to the bottom. Within several minutes, the cell was filled with many needle-like crystals (Figure 4).

Because the time between stages (a) and (c) in Figure 4 is approximately that of the exothermal event in Figure 3, the latter event was probably a crystallization process like stage (d) in Figure 4. Therefore, we defined the induction time for hydrate nucleation as the time interval between the introduction of CO_2 into the high-pressure cell to the measured temperature rise (see Figure 3). This definition of the induction time includes the time for CO_2 to diffuse into the water as discussed in a section IVa.

b. Nucleation Probability Distribution. To obtain the nucleation probability distribution for each preparation method,

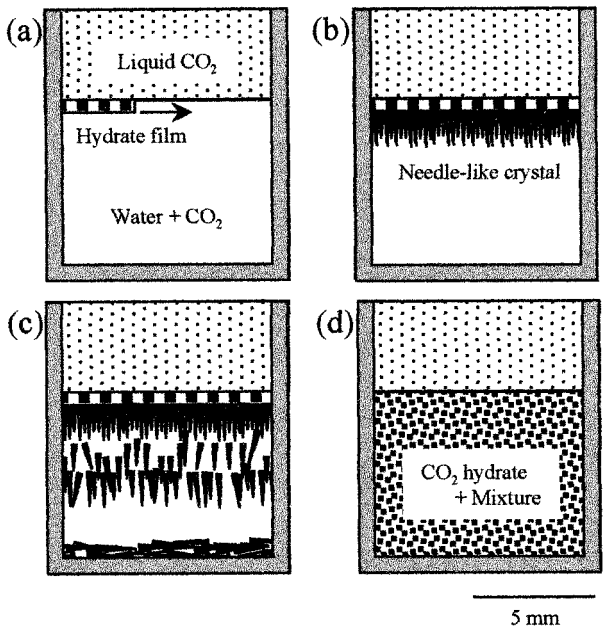

Figure 4. Illustration of CO_2 hydrate formation based on experiments with a transparent cell. (a) A thin film cross the CO_2−H_2O boundary within a second. (b) Growth of needle-like crystals within several tens of seconds. (c) Needle-like crystals fall. (d) Mixture filled with crystals within several minutes.

we repeated the induction time measurement 10 times under the same experimental conditions, each time using a new sample. Using the induction time t_m measured for the mth shortest induction time among the 10 measurements, the nucleation probability distribution $P(t)$ that nucleation occurred on or before time t_m is given by $P(t_m) = m/10$. When the CO_2 hydrate did not nucleate within 5 days, we stopped the measurement.

The nucleation probability distribution of four kinds of water samples, nontreated water, meltwater, degassed water, and degassed meltwater, are plotted against the logarithm of the time in Figure 5a. The shortest induction times for each water sample are nearly the same for nontreated water and meltwater, degassed water and degassed meltwater, respectively, but the distribution of the induction times depends on the water samples.

According to nucleation theory,[12] the nucleation probability distribution $P(t)$ can be expressed by a nucleation rate J in a given volume of liquid as

$$P(t) = 1 - \exp\{-J(t - \tau_0)\} \quad (1)$$

where τ_0 is an onset time of nucleation. The parameters J and τ_0 were obtained by fitting eq 1 with the nucleation probability data for the four different water samples and are tabulated in Table 1. Freezing−melting caused J to increase by a factor of 7.8, whereas degassing caused J to decrease by a factor of 2.5. We have no explanation for this coincidence.

We then examined the effect of heating meltwater on J by keeping the meltwater sample at 298 K for 1 h after procedure (2) for freezing, but before introducing CO_2. The induction times for the heated meltwater samples are much longer on average than those for the meltwater and nontreated water: the freezing-memory effect vanished after heating (Figure 5b).

Finally, we investigated the effects of saturating the water with several different dissolved gases. Figure 5c indicates that only dissolved O_2 increased the nucleation rate; N_2 and CO_2 instead decreased the nucleation rate.

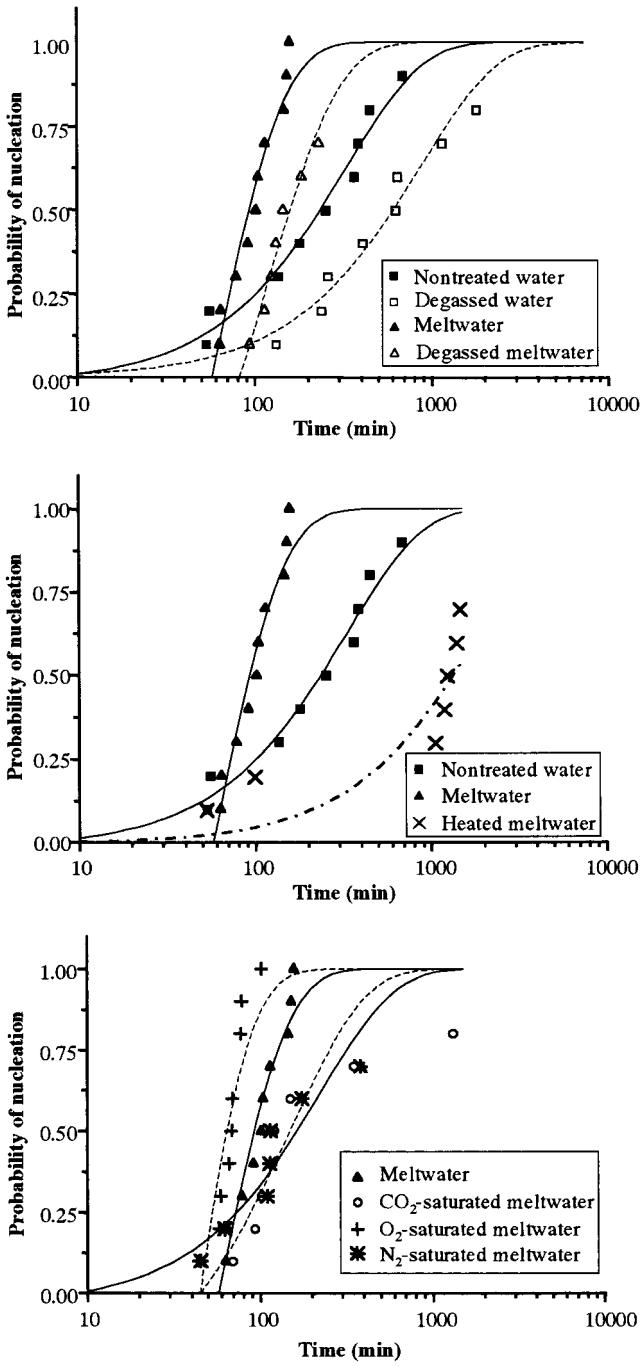

Figure 5. (a) Nucleation probabilities versus reaction time for different water samples. (b) Nucleation probabilities versus reaction time for nontreated water, meltwater, and heated meltwater. The data of nontreated water and meltwater are identical with those of Figure 5a. (c) Nucleation probabilities versus reaction time for meltwater, O_2-saturated meltwater, N_2-saturated meltwater, and CO_2-saturated meltwater. The data of meltwater are identical with those of Figure 5a.

TABLE 1: Nucleation Rates for Various Waters

	τ_0 (min)	J (min^{-1})
nontreated water	7.9	2.95×10^{-3}
meltwater	58.8	2.29×10^{-2}
degassed water	27.1	1.18×10^{-3}
degassed meltwater	81.6	9.16×10^{-3}
O_2-saturated meltwater	44.9	3.60×10^{-2}

IV. Discussion

a. Dissolution of Gases into Water. In the present study, CO_2 molecules diffuse into the water under quiescent conditions. The water at the CO_2−water boundary immediately saturates with CO_2; water below the boundary will gradually saturate with CO_2 depending on the distance from the boundary. Assuming the CO_2 interdiffusion coefficient in water at 273 K and 5 MPa is 9.6×10^{-10} m^2/s[13] and ignoring natural convection, we estimate that it takes about 100 s to saturate water with CO_2 in the water layer at a distance of 3 mm below the boundary.[14] Uchida et al.[11] reported that CO_2 hydrate films grow mainly into the water phase at the boundary between CO_2 and water. Using a heat diffusion model, they estimated the film thickness to be 0.13 μm for temperatures between 268.2 and 288.2 K and pressures between 1.8 and 7.2 MPa. Assuming this thickness, we estimate that it took less than one millisecond to saturate water with CO_2 where the hydrate film grew.

When the CO_2 hydrate nucleated, the water just below the hydrate film might be saturated with CO_2: a condition supersaturated with respect to the hydrate.[15] Therefore, the CO_2 hydrate could grow rapidly into the water until the mixture equilibrated with CO_2 hydrate. Thus, despite the CO_2−H_2O boundary being covered by a hydrate film (Figure 4b), crystal growth would continue after the first needle-like crystals grew into the water.

The number concentration of CO_2 molecules in water at 4.7 MPa and 273 K, extrapolated from 2.9 MPa and 273 K[16] is 2×10^{22} mol^{-1}. Here, we used the experimental result for CH_4 (Lekvam and Bishnoi[17]). The saturated concentration of N_2 and O_2 in water at atmospheric pressure and 273 K are estimated from their partial pressures and solubilities at atmospheric pressure:[18] $[N_2] = 9 \times 10^{18}$ mol^{-1}, $[O_2] = 5 \times 10^{18}$ mol^{-1}, $[CO_2] = 2 \times 10^{17}$ mol^{-1}. Therefore, the number concentration of N_2, O_2, and CO_2 molecules in N_2-saturated water, O_2-saturated water, and CO_2-saturated water at 0.1 MPa and 273 K are estimated to be 1×10^{19}, 2×10^{19}, and 8×10^{20} mol^{-1}, respectively. Therefore, our experimental results showed that although dissolved O_2 molecules are a factor of 40 less than CO_2, they significantly affected CO_2 hydrate nucleation.

b. Nucleation Mechanisms. Because the nucleation rate of a crystal is usually controlled by impurities or surfaces (heterogeneous nucleation), there are various possible mechanisms to consider. Nucleation might have occurred on the vessel wall near the CO_2−water boundary, or on a small particle. The energy barrier for nucleation of a crystal in a liquid phase, the crystal-liquid interfacial energy, must be overcome by an aggregation of a sufficiently large number of molecules to form a nucleus larger than a critical size. A surface or particle can provide a supercritical size and reduce the effect from the interfacial energy. Thus, the vessel wall or dissolved impurity is favorable for the nucleation by this heterogeneous effect.

The freezing-memory effect found in the present study suggests that a particular substance or structure exists in water, or on the wall after melting from ice. Because the freezing-memory effect vanished by heating the meltwater sample, this substance or structure is metastable; it is neither the small cracks in the vessel wall nor dissolved impurity. Because the nucleation rates decreased by degassing, and increased with the O_2 concentration in water, this particular substance or structure is probably composed of gaseous molecules such as O_2, although we have no direct evidence for such a structure in water.

A possible structure is a metastable polyhedral water cluster encaging an O_2 molecule such as a 12-hedral cage of the O_2 hydrate (structure II). If such polyhedral clusters are formed in water or on the vessel wall by freezing followed by melting, the nucleation rate of the CO_2 hydrate crystals could increase by the aggregation of these clusters to form the hydrate structure.

Our experimental result implies a polyhedral cluster lifetime greater than 2 h at 275 K. And, the nucleation of CO_2 hydrate could be extremely sensitive to such small cluster concentrations.

V. Summary

Nucleation rates of CO_2 hydrate crystals were measured for water samples prepared by different treatments. Because the nucleation rate using water from melted ice was 1 order of magnitude larger than that from nonfrozen water, we proposed a freezing-memory effect of water on nucleation. This effect vanished when the meltwater sample was heated to 298 K, but was enhanced by saturating the water with O_2. These experimental results could be explained if the meltwater contains long-lived metastable water clusters encaging O_2 molecule that were transferred from the ice, or if a clathrate-like structure remains in solution with a long lifetime greater than 2 h after ice melts under 275 K.

References and Notes

(1) Stackelberg, M. V.; Muller, H. R. *Naturwiss*. **1951**, *38*, 456.
(2) Muller, H. R.; Stackelberg, M. V. *Naturwiss*. **1952**, *39*, 20.
(3) Vysniauskas, A.; Bishnoi, P. R. *Chem. Eng. Sci*. **1983**, *38*, 1061.
(4) Parent, J. S.; Bishnoi, P. R. *Chem. Eng. Comm.* **1996**, *144*, 51.
(5) Hwang, M. J.; Wright, D. A.; Kapur, A.; Holder, G. D. *J. Inclusion Phenom.* **1990**, *8*, 103.
(6) Sloan, E. D.; Subramanian, S.; Matthews, P. N.; Lederhos, J. P.; Khokhar, A. A. *Ind. Eng. Chem. Res.* **1998**, *37*, 3124.
(7) Schroeter, J. P.; Kobayashi, R.; Hidebrand, M. A. *Ind. Eng. Chem. Fundam*. **1983**, *22*, 361.
(8) Benmore, C. J.; Soper, A. K. *J. Chem. Phys*. **1998**, *108*, 6558.
(9) Sloan, E. D. *Clathrate Hydrate of Natural Gases*, 2nd ed.; Marcel Dekker Inc.: New York, 1998; Chapter 3.
(10) Koh, C. A.; Savidge, J. L.; Tang, C. C. *J. Phys. Chem*. **1996**, *100*, 6412.
(11) Uchida, T.; Ebinuma, T.; Kawabata, J. *J. Cryst. Growth* **1999**, *204*, 525.
(12) Toschev, S.; Milchev, A.; Stoyanov, S. *J. Cryst. Growth* **1972**, *13*/*14*, 123.
(13) Funazukuri, T.; Nishio, M. *Kagaku Kogaku Ronbunshu* **1995**, *21*, 824.
(14) Crank, J. *The mathematics of diffusion*, 2nd. ed.; Clarendon Press: Oxford, 1975; Chapter 4.
(15) Yamane, K.; Aya, I. MARIENV '95 (Proceedings of the International Conference on Technologies for Marine Environmental Preservation), Tokyo; Society of Naval Architects of Japan: Tokyo, 1995; vol. 2, p 911.
(16) Stewart, P. B.; Munjal, P. *J. Chem. Eng. Data* **1970**, *15*, 67.
(17) Lekvam, K.; Bishnoi, P. R. *Fluid Phase Equilib*. **1997**, *131*, 297.
(18) Lide, D. R., Ed.*CRC Handbook of Chemistry and Physics*, 77th ed.; CRC Press. Inc.: Boca Raton, FL, 1996−1997.